

Slim-neck by GSConv: A better design paradigm of detector architectures for autonomous vehicles

Hulin Li^{1,*}, Jun Li², Hanbing Wei², Zheng Liu³, Zhenfei Zhan² and Qiliang Ren¹

¹ College of Traffic and Transportation, Chongqing Jiaotong University, Chongqing 400074, China

² School of Mechatronics and Vehicle Engineering, Chongqing Jiaotong University, Chongqing 400074, China

³ School of Engineering, University of British Columbia, Okanagan, Kelowna BC V1V 1V7, Canada

* Correspondence

AlanLi@mails.cqjtu.edu.cn (H.L.); cqleejun@163.com (J.L.); hbwei@cqjtu.edu.cn (H.W.); zheng.liu@ubc.ca;

Zhenfei_zhan@163.com (Z.Z.); cqrql@126.com (Q.R.)

Abstract

Object detection is a difficult downstream task in computer vision. For the on-board edge computing platforms, a giant model is difficult to achieve the real-time detection requirement. And, a lightweight model built from a large number of the depth-wise separable convolutional layers cannot achieve the sufficient accuracy. We introduce a new method, GSConv, to lighten the model but maintain the accuracy. The GSConv balances the model's accuracy and speed better. And, we provide a design paradigm, slim-neck, to achieve a higher computational cost-effectiveness of the detectors. In experiments, our method obtains state-of-the-art results (e.g. 70.9% mAP_{0.5} for the SODA10M at a speed of ~100FPS on a Tesla T4) compared with the original networks. Code will be open source at <https://github.com/AlanLi1997/Slim-neck-by-GSConv>

1. Introduction

Object detection is a fundamental perception capability required for driverless cars. Currently, detection algorithms by deep learning dominate the field. These algorithms are of two types in terms of detection stages: the one-stage [1-3] and the two-stage [4-9]. The two-stage detectors perform better in the detection of small objects and get higher mean average precision (mAP) by the principle of sparse detection, but these detectors all come at the cost of speed. The one-stage detectors are not as effective as two-stage detectors in the detection and localization of small objects, but they are faster than the latter on work, which is very important for industry. The intuitive understanding from brain-like research is that the model with more neurons gain a stronger nonlinear expression ability. But what should not be neglected is that the powerful ability and low energy consumption of the biological brains to process information are beyond the computers far. We cannot build the strong model by simply increasing the number of model parameters endlessly. The lightweight design is effective to mitigate high computational costs at the current stage. This purpose is mostly accomplished by using the depth-wise separable convolution (DSC) operations to reduce the amounts of parameters and FLOPs, and the effect is obvious, details in Appendix.

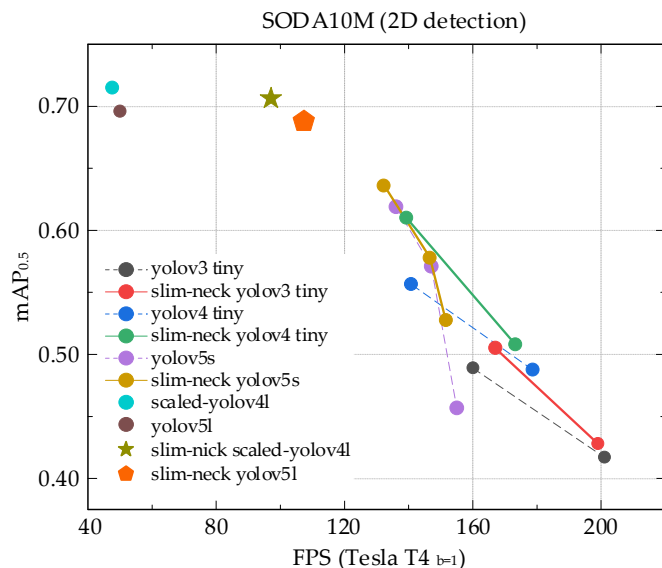


Figure 1. The comparison of the slim-neck YOLO family detectors and the originals.

However, the disadvantages of the DSC are also obvious: the channel information of the input image is separated in the calculation process.

For self-driving cars, the speed is as important as the accuracy. We introduce the new method of slim neck by the GSConv to lighten the model but maintain the accuracy. The GSConv balances the model's accuracy and speed better. In Figure 1, we compare the speed and accuracy of the slim neck state-of-the-art detectors and the originals on the driverless dataset of the SODA10M. The results confirm the effectiveness of this method. Figure 2 (a) and (b) show the calculation process of the DSC and the standard convolution (SC). This deficiency results the DSC in a much lower feature extraction and fusion capability than the SC. The excellent lightweight works, such as Xception [10], MobileNets [11-13] and ShuffleNets [14-15], improved the detector speed greatly by the DSC operations. But the lower accuracy of these models is worrying when these models are applied to the autonomous vehicles. In fact, these works propose some methods to alleviate this inherent flaw (it is also a peculiarity) of the DSC: MobileNets use a large number of 1*1 dense convolutions to fuse the channels information that is computed independently; ShuffleNets use the "channel shuffle" to enable the interaction of channels information and GhostNet [16] uses "halved" SC operations to retain the

interaction information between channels. But, the 1*1 dense convolutions take up more computational resources instead, the effect of using “channel shuffle” still does not touch the results of the SC and the GhostNet is more or less back on the road to the SC, influences may come from many aspects. Many lightweight models use the similar thinking to design the basic architecture: only use the DSC from the very beginning to end of the deep neural networks. But the DSC’s flaw is directly amplified in the backbone, whether this is used for image classification or detection. We believe that the SC and the DSC can be cooperative. We note that the feature maps generated by only shuffling the output channels of the DSC are still “depth-wise separated”. In order to make the outputs of the DSC as close as possible to the SC, we introduce a new method-GSConv. As show in Figure 3, we use the shuffle to permeate the information generated by the SC (the dense convolution operations) into every part of the information generated by the DSC. This method allows the information from the SC to be fully mixed into the outputs of the DSC, without bells and whistles. Figure 4 shows the visualization results of the SC, DSC and GSConv. The GSConv’s feature maps are significantly more similar to the SC’s than the DSC’s is to the SC’s. When we use the SC in the backbone and use the GSConv in the neck (slim-neck), the accuracy of the model is very close to the original; and if we add a few tricks, the accuracy and speed of the model surpass the original model. The slim-neck with GSConv method minimizes the negative impact of the DSC’s flaw on the models and to utilize the benefits of the DSC efficiently. The main contributions of ours can be summarized as follows:

1. We introduce a new method, the GSConv, to replace the SC operation. This method makes the outputs of the convolution calculation as close to the SC’s as possible, and reduces the computational cost;
2. We provide a design paradigm, slim-neck with standard backbone, for the detector architecture of self-driving cars;
3. We verified the effectiveness of different widely used tricks, which can be a reference for study in this field.

The rest of the article is organized as follows: we give a brief overview of some relevant works and methods about the lightweight and performance improvement of detectors in Section 2, and provide the details of our study in Section 3, our experimental results presented in Section 4, all the work summarized with a final conclusion in Section 5.

2. Related Work

Usually, a detector based on the convolutional neural networks (CNNs) consists of three parts, a backbone, a neck and a head. The backbone for the extraction features of the input, the neck for allocation and merging features better to the head, and the head detects the objects by materials from the neck. For the backbone, AlexNet [17] demonstrated the powerful feature extraction ability of CNNs. Then, the backbone of detectors or

classifiers started to be designed using standard convolutions, such as VGG [18], ResNet [19] and DarkNet [6-7]. However, these “bulky” models are very unfriendly to edge computing devices. In terms of model structure design, researchers have proposed classic lightweight models such as MobileNet, ShuffleNet, and GhostNet for edge devices. For the neck, FPN [20] improves the speed and accuracy of object detection models by independently performing prediction operations on different scale feature map layers. For the head, the main difference is that the model uses anchor-based [1-3, 5-9] or anchor-free [21-22] methods to accomplish objects localization tasks. The former may be more controllable for designers and users, but the NMS [23] must be used to filter out the prediction box with the highest IOU threshold score. The latter is more flexible and no more parameters can be controlled manually, but this also leads to an increase in instability of the model. The choice of anchor-based or anchor-free is not the focus of this paper, but it is worth noting that the SOTA model, Scaled-YOLOv4 [24], is still using the anchor-based method currently. More, the attention mechanisms, such as SPP [25], SE [26], CBAM [27] and CA [28], can improve the efficiency and performance of detectors, especially for the lightweight detectors. We can obtain the better cost performance by a proper use of these modules, and the relevant details are described in Section 3.

3. Materials and Methods

The details of our work will be described in this section. We aim to build a simple and efficient neck for the detectors to apply in the autonomous vehicles. Therefore, many factors such as convolution method, feature fusion structure, computational efficiency, computational cost effectiveness and many other factors are taken into our considerations.

3.1. Why using the GSConv in the neck

In order to speed up the computation of predictions, the fed images in CNNs almost always have to undergo a similar transformation process in the backbone: the spatial information is transferred step by step toward the channels. And each time the spaces (the width and height) compression and channels expansion of the feature maps will cause a partial loss of semantic information. The dense convolutional computation maximally preserves the hidden connections between each channel, but the sparse convolution severs these connections completely. The GSConv preserves these connections as much as possible. But if we use it at all stages of the model, the model’s network layers will be deeper and deep layers will aggravate the resistance to data flow and increase the inference time significantly. When these feature maps come to the neck, they have become slender enough (the channel dimension reaches the maximum, and the width and height dimensions reach the minimum) and no longer need to be transformed. So, the better choice is to use the GSConv in the neck only (slim-neck + standard backbone). At this stage, using the GSConv to process the

concatenated feature maps is just right: redundant repetitive information is less and compressed not needed, and the attention modules works better, such as the SPP and the CA.

3.2. The slim-neck

We investigate the generalized methods to enhance the learning ability of CNNs, such as DensNet [29], VoVNet [30] and CSPNet [31], and then design the structure of slim-neck on the theory of these methods.

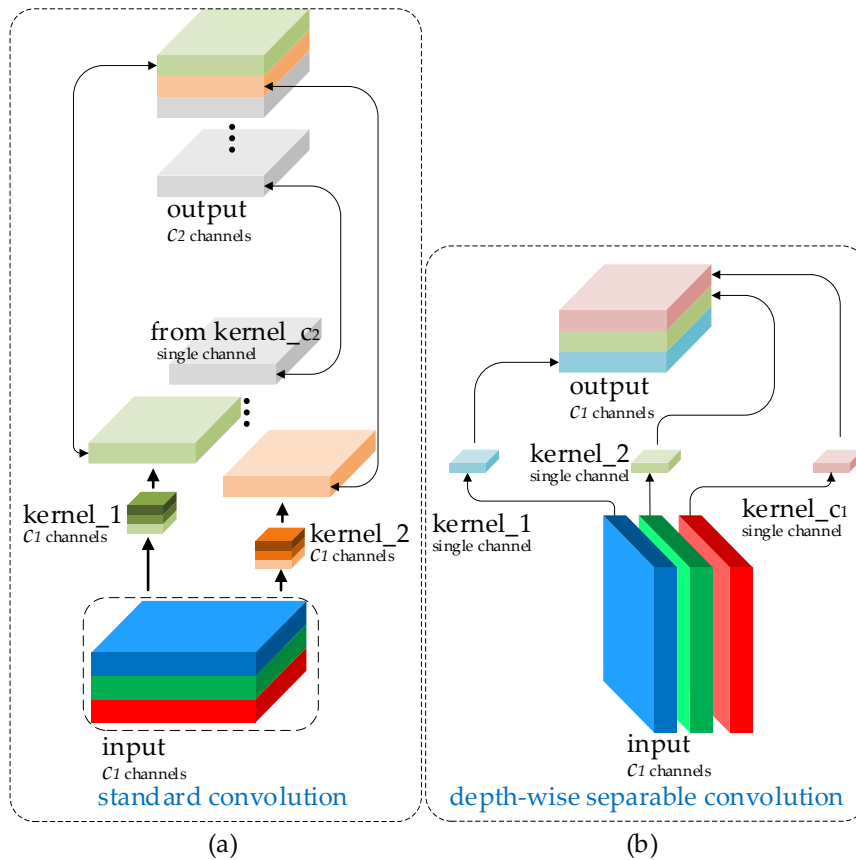


Figure 2. The calculation process of the (a) SC and the (b) DSC. The SC is the dense convolution computation and the DSC is the sparse convolution computation.

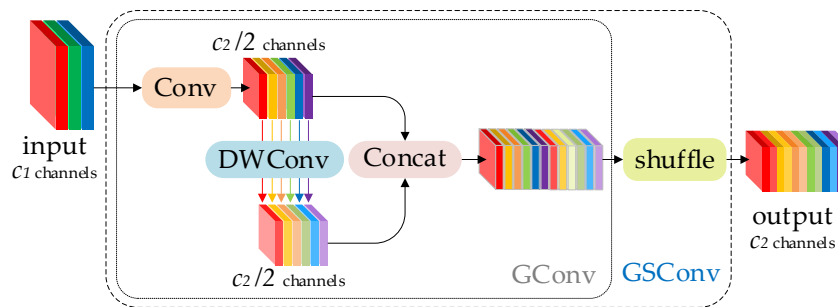


Figure 3. The structure of the GSConv module. The “Conv” box consists of three layers: a convolutional-2D layer, a batch normalization-2D layer, and an activation layer. The “DWConv” marked in blue here means the DSC operation.

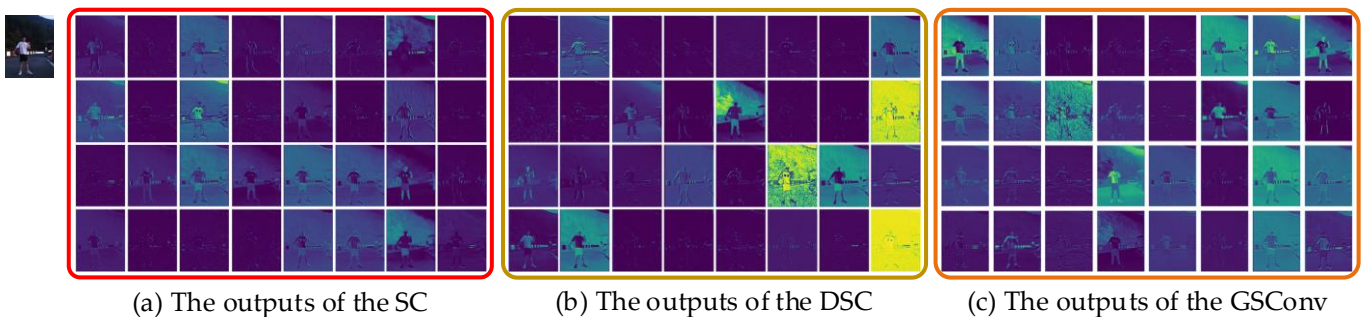


Figure 4. The feature maps in the 2nd layer of the YOLOv5n. (a) The feature maps generated by the SC operation. (b) The feature maps generated by the DSC operation. (c) The feature maps generated by the GSConv operation.

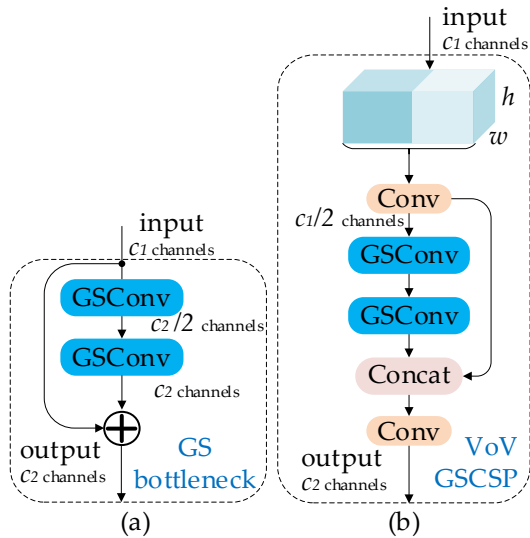


Figure 5. The structures of the (a) GS bottleneck module and the (b) VoV-GSCSP module.

3.2.1. The element modules of the slim-neck

First, we use the GSConv, a lightweight convolution method, to replace the SC. Its computational cost is about 60%~70% of the SC, but its contribution to the model learning ability is comparable to the latter. Then, we continue to introduce the GS bottleneck on the basis of the GSConv, and Figure 5 (a) shows the structure of the GS bottleneck module.

Again, we use the one-shot aggregation method to design the cross stage partial network (GSCSP) module, VoV-GSCSP. The VoV-GSCSP modules reduce the computational and network structure complexity but maintain the sufficient accuracy. Figure 5 (b) shows the structure of the VoV-GSCSP. It is worth noting that if we use the VoV-GSCSP to replace the CSP in the neck, where the CSP layer consists of the standard convolution, the FLOPs will be on average 15.72% less than latter.

Finally, we need the flexibility to use the four modules, the GSConv, the GS bottleneck, and the VoV-GSCSP. We can build the slim-neck layers like to put together Legos.

3.2.2. The slim-neck for the YOLO family

The YOLO family detectors are more widely used in the industry because of the efficient detection. We use the element modules of the slim-neck to retrofit the neck layers for the Scaled-YOLOv4 and YOLOv5. Figure 6 and 7 show the two slim-neck architectures.

3.3. The improvement tricks for free

We can use some local feature enhancement methods in CNNs-based detectors with simple structure and low computational cost. These enhancement methods, attention mechanisms, can significantly improve the model accuracy, but are much cheaper than the neck. These methods include acting on channel information or acting on spatial information. The SPP focuses on spatial

information, which is concatenated of four parallel branches: three maximum pooling operations (kernel size is 5×5, 9×9 and 13×13) and a shortcut from the input. It is used to solve the problem of the excessive object scale variations, by merging the local and global features of the inputs. The SPPF, the SPP improved module by the YOLOv5’s author, enhances the computational efficiency. This efficiency, η_c , increased by nearly 277.8%. And the general formula of the η_c is:

$[(k_1^2 + k_2^2 + k_3^2 + \dots + k_i^2 - i) - (k_1^2 - 1) \times i] \times 100\%$, where k_i is the kernel size of the i -th branch of maxpooling-2D in SPPF module. Figure 8 (a) and (b) show the structures of the SPP and SPPF. The SE is a channel attention module, including two operation processes: the squeeze and the excitation. This module allows the networks to focus more on the more informative features channels and negatives the less informative features channels. The CBAM is a spatial-channel attention mechanism module. The CA module is a new solution to avoid the loss of positional information caused by global pooling-2D operation: to put the attention in two dimensions of width and height respectively for the efficient utilization of the spatial coordinate information of input feature maps. Figure 9 (a), (b) and (c) show the structures of the SE, CBAM and CA module.

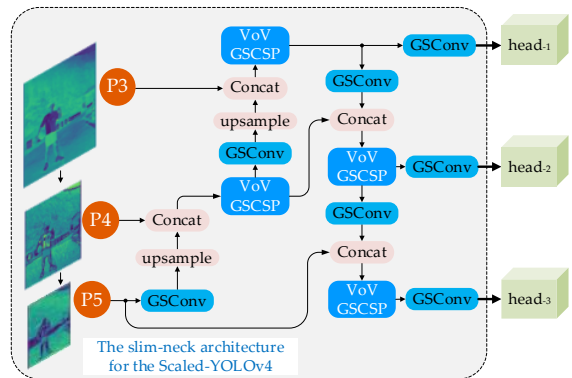


Figure 6. The slim-neck architecture for the Scaled-YOLOv4(p5).

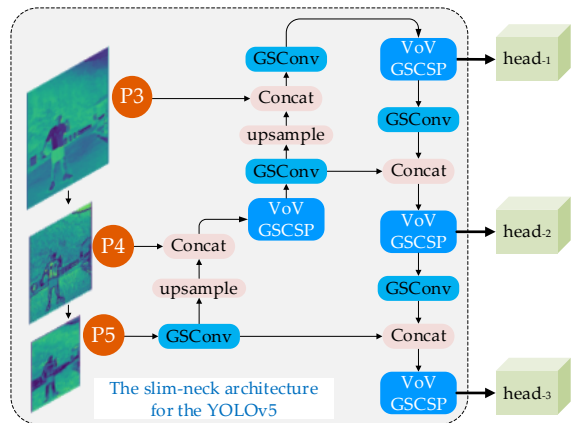


Figure 7. The slim-neck architecture for the YOLOv5.

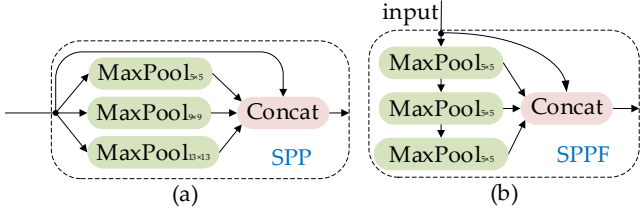


Figure 8. The structures of the (a) SPP module and (b) SPPF module. The SPPF’s output is the same as SPP’s with more computationally efficient.

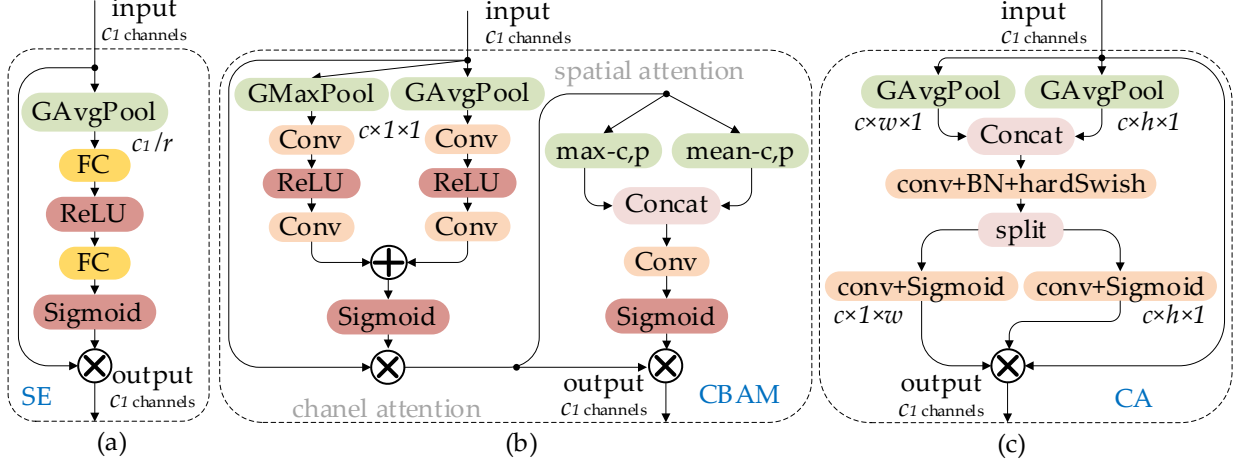


Figure 9. The structures of the three different attention modules. (a) The SE module, the character “GAvgPool” means the global average pooling-2D layer, the character “FC” means the fully connection layer, and the “r” is a reduction factor. (b) The CABM module, the character “Conv” means the ordinary convolution-2D layer, and the “max-c, p” and “mean-c, p” means the maximum-channel-pixel and average-channel-pixel. (c) The CA module, the character “BN” means the batch normalization layer and the character “hardSwish” means the hard-Swish activation layer.

3.4. The Loss and Activation

The IoU [32] loss plays a great value for the detectors based on deep learning. It makes the location of prediction bounding boxes regression more accurate. As research continues to evolve, more advanced IoU loss functions have been proposed by a number of researchers, such as GIoU [33], DIoU [34], CIoU [35] and the latest EIoU [36]. The five loss functions are defined as follows:

$$Loss_{IoU} = 1 - IoU, \quad IoU = \frac{A \cap B}{A \cup B} \quad (1)$$

$$Loss_{GIoU} = 1 - IoU + \frac{C - (A \cup B)}{C} \quad (2)$$

$$Loss_{DIoU} = 1 - IoU + \frac{\rho_{(b,b^{gt})}^2}{d^2} \quad (3)$$

$$Loss_{CIoU} = 1 - IoU + \frac{\rho_{(b,b^{gt})}^2}{d^2} + \alpha v,$$

$$\alpha = \frac{v}{(1 - IoU) + v}, \quad v = \frac{4}{\pi^2} (\arctan \frac{w^{gt}}{h^{gt}} - \arctan \frac{w}{h})^2 \quad (4)$$

$$Loss_{EIoU} = 1 - IoU + \frac{\rho_{(b,b^{gt})}^2}{d^2} + \frac{\rho_{(w,w^{gt})}^2}{C_w^2} + \frac{\rho_{(h,h^{gt})}^2}{C_h^2} \quad (5)$$

where the parameters “A” and “B” denote the area of ground truth bounding box and the area of prediction bounding box; the parameter “C” denotes the area of the minimum enclosing box of the ground truth bounding box and the prediction bounding box; the parameter “d”

One suggestion is that the attention modules are usually placed at the end of the backbone to achieve better results, while the simple but effective SPPF module can be directly embedded at the entrance of the head. This is because the shallow networks are flooded with a large amount of low-level semantic information, resulting in the information fusion function of the attention modules being of minimal use: it is completely unnecessary to fuse feature maps that already contain rich low-level semantic information

denotes the Euclidean distances of the diagonal vertices of the enclosing box; the parameter “ ρ ” denotes the Euclidean distances of the centroids of ground truth bounding box and prediction bounding box; the parameter “ α ” is an indicator for trade-off, and the parameter “v” is an indicator to evaluate the consistency of the aspect ratio of the ground truth bounding box and prediction bounding box.

The CIoU loss is currently the most widely used loss function in anchor-based detector, but there are still flaws in the CIoU loss:

$$\frac{\partial v}{\partial w} = \frac{8}{\pi^2} (\arctan \frac{w^{gt}}{h^{gt}} - \arctan \frac{w}{h}) \times \frac{h}{w^2 + h^2},$$

$$\frac{\partial v}{\partial h} = -\frac{8}{\pi^2} (\arctan \frac{w^{gt}}{h^{gt}} - \arctan \frac{w}{h}) \times \frac{w}{w^2 + h^2} \quad (6)$$

where the “ $\partial v / \partial w$ ” is the gradient of the “v” with respect to the “w”, the “ $\partial v / \partial h$ ” is the gradient of the “v” with respect to the “h.”

According to the definition of the CIoU loss, if $\{(w = kw^{gt}, h = kh^{gt}) | k \in R^+\}$, the CIoU loss will degenerate into the DIoU loss, i.e., the relative proportion of penalty terms added in the CIoU loss (αv) will not work. Further, the $\partial v / \partial w$ and the $\partial v / \partial h$ have opposite signs, $\partial v / \partial w = -(h/w) \times (\partial v / \partial h)$. Thus, these two variables (w or h) can only be updated in the same direction, increasing or decreasing at the same time. This is not in line with practical application scenarios especially when $w < w^{gt}$

and $h < h^{st}$ or $w > w^{st}$ and $h > h^{st}$. The EIoU loss does not face such a problem, it directly uses the w and h of a prediction bounding box independently for the penalty term, instead of the ratio of the w and h . Figure 10 are three examples of the different evaluation indicators of these loss functions.

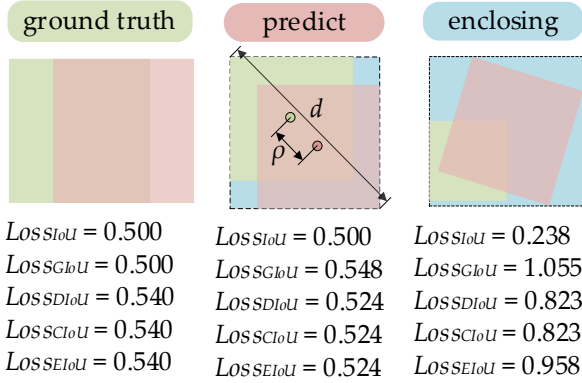


Figure 10. The comparison of three examples of five different loss functions evaluation indicators.

On deep networks, the accuracy and training stability of the models using Swish [37] and Mish [38] are generally better than ReLU [39]. Both the Swish and Mish have the properties of no upper bound with lower bound, smooth, and non-monotonic. They are defined as follows:

$$\text{Swish: } f(x) = x \cdot \text{sigmoid}(\beta x) \quad (7)$$

$$\text{Mish: } f(x) = x \cdot \tanh(\log(1 + e^x)) \quad (8)$$

The Mish performs slightly better for model accuracy than Swish on deeper networks, although in fact the two activation function curves are so close. Compared with the Swish, the Mish consumes more training time because of the increase in computational cost. We performed adequate ablation experiments to verify the effectiveness of these methods. The comparative analyses are reported in Section 4.

4. Experiments and Analysis

We use the Pytorch framework to build the models. All the models are trained with two Tesla T4 GPUs at Linux CentOS 7 operating system. The hyper-parameters

are as follows: the training steps is 33000; the optimizer is stochastic gradient descent (SGD); the batch size is 128; the linear decay learning rate scheduling strategy is adopted with initial learning rate 0.01 and final 0.001; the warm-up steps is 1128; the momentum and weight decay are 0.937 and 0.0005. All the validation experiments are performed on a Tesla T4 or a Jetson Nano.

4.1. Data Sets

We use the publicly available data sets WiderPerson [40], PASCAL VOC [41] and SODA10M [42]. We choose the WiderPerson to evaluate the practical effects of the GSConv method and the different attention modules. It is a pedestrian detection benchmark dataset in the wild, of which images are selected from a wide range of scenarios, no longer limited to the traffic scenario. The images collected in this dataset are all in a dense crowded environment with a large number of pedestrians and serious overlap and mutual occlusion. And, we use the PASCAL VOC 2007+12 to compare with the state-of-the-art lightweight models. Ultimately, we use the SODA10M to test the real-world performance of these models in a traffic environment. We test the evolved models on a Jetson Nano, and on the low-power edge devices we expect these models to be competent for the use cases in embedded or IoT scenarios.

4.2. Results Discussion

The experimental results of the employing different attention modules by the YOLOv5n are reported in TABLE 1. All the models in the part 1 use the slim-neck with slim-backbone, and the models in the part 2 only use the slim-neck. The experimental datasets are the WiderPerson and VOC 2007+12. In TABLE 1, the "SE*3₆₄₀" indicates that the SE module is used three times and SPPF once in the YOLOv5n's structure, and the training image size is 640×640 pixels; mAP_{0.5} is the average precision of the all categories when the accuracy evaluation IoU threshold is set to 0.5 and mAP_{0.95} is the average precision with the IoU threshold taken in steps of 0.05 from 0.5 to 0.95 and weighted average.

Table 1. The performance comparisons of employment of different attention modules.

Attention modules	Parameters number (million)	Precision / Recall	mAP _{0.5}	mAP _{0.95}	Inference time _{b=64} (ms)	FLOPs
Part I. slim-backbone + slim-neck						
WiderPerson _{single class: pedestrian}						
SE*3 ₆₄₀	0.664	63.5 / 78.8%	79.9%	46.4%	2.2	1.7B
CBAM*3 ₆₄₀	0.664	63.8 / 79.0%	79.9%	46.4%	2.3	1.7B
CA*3 ₆₄₀	0.665	56.6 / 82.0%	80.4%	47.1%	2.2	1.7B
PASCAL VOC 2007+12 _{20 classes}						
SE*3 ₆₄₀	0.685	57.3 / 52.3%	51.4%	27.5%	2.3	1.8B
CBAM*3 ₆₄₀	0.685	59.8 / 51.1%	51.2%	27.7%	2.4	1.8B
CA*3 ₆₄₀	0.685	58.5 / 52.3%	52.1%	28.6%	2.3	1.8B
Part II. slim-neck only						
WiderPerson _{single class: pedestrian}						

SE*3 ₆₄₀	1.14	62.3 / 82.9%	82.7%	50.6%	1.7	3.5B
CBAM*3 ₆₄₀	1.14	64.1 / 81.4%	82.1%	49.9%	1.9	3.5B
CA*3 ₆₄₀	1.14	60.5 / 84.4%	83.3%	51.5%	1.9	3.5B
PASCAL VOC 2007+12 _{20 classes}						
SE*3 ₆₄₀	1.17	64.2 / 56.9%	59.2%	37.6%	2.2	3.5B
CBAM*3 ₆₄₀	1.17	61.4 / 58.2%	58.7%	36.8%	2.3	3.5B
CA*3 ₆₄₀	1.17	64.2 / 57.5%	59.3%	38.3%	2.3	3.5B

We found that the effect of different attention modules on the number of parameters and inference time of the detector is so slight as to be almost negligible but the impact on the accuracy is significant. In TABLE 1, the “CA*3+SPPF*1” model obtains the best results on the VOC 2007+12 and WiderPerson datasets. In addition, the accuracy of the slim-neck model is much better than that of the slim-backbone-neck when the inference time is very close. If we force to close the accuracy of the slim-neck model and the slim-neck-backbone model, the latter needs to spend more than 3.5% inference time.

Further, we conducted comparative experiments on the effects of Mish and Swish activation functions, as well as CIoU and EIou loss functions for accuracy and speed. In TABLE 2, we reported the experimental results on the VOC 2007+12 dataset. The networks using Mish with EIou achieve the higher average accuracy, while the networks using Swish achieve the faster speed (training time

using the Mish increases by about 29.26% than Swish). For contrast intuitive, we validated the effectiveness of our method with YOLOv5n as a baseline, and TABLE 3 reported the relevant experiment results.

Finally, we give the performance comparisons of the slim-neck YOLO detectors and the originals in TABLE 4. The slim-neck detectors achieve the best accuracy with the smaller size. The combination of the slim-neck method and the tricks makes a huge improvement on the accuracy, especially to the lightweight detectors such as the YOLOv3/v4-tiny. And we put slim-neck tiny detectors on the Jetson Nano embedded device for inferring with 320×320 pixels, results listed in TABLE 5. We test the effectiveness of our approach using a 20-second field video that was captured by a dash cam at night in low-light. In Figure 11, we show four frames from the test video as an intuitive comparison.

Table 2. The comparison of the effects of Swish/Mish activation functions and CIoU/EIoU loss functions (dataset: PASCAL VOC 2007+12).

Attention modules	Activation / Loss function	mAP _{0.5}	mAP _{0.95}	Inference time _{b=1} (ms)	FPS
	Swish, CIoU	59.3%	38.3%	5.8	136.4
CA*3, SPPF*1 ₆₄₀ (slim-neck only)	Swish, EIou	59.7%	38.5%	5.7	138.4
	Mish, CIoU	60.0%	38.4%	7.0	119.0
	Mish, EIou	60.6%	39.1%	7.2	116.3

Table 3. The ablation studies of three implements: the slim-neck, attention modules, and activation & loss functions (dataset: PASCAL VOC 2007+12). Models marked ‘*’ are the more cost-effective.

Model	Parameters number / FLOPs	mAP _{0.5}	mAP _{0.95}	Inference time _{b=1} (ms)	FPS
Baseline (YOLOv5n)	1.79M, 4.3B	58.0%	35.0%	5.8	136.8
Baseline + slim-backbone-neck	0.67M(-63%), 1.8B	51.5%(-6.5)	27.9%(-8.1)	5.0	151.9
Baseline + slim-backbone-neck (deep)	1.23M(-31%), 4.0B	61.1%(+3.1)	39.7%(+4.7)	6.0	132.7
Baseline + slim-neck *	1.15M(-36%), 3.5B	58.9%(+0.9)	37.1%(+2.1)	4.8	155.4
Baseline + slim-neck, SPPF*1, CA*3, Mish, EIou	1.17M(-36%), 3.5B	60.6%(+2.6)	39.1%(+4.1)	7.2	116.3
Baseline + slim-neck, SPPF*4, CA*3, Mish, CIoU	1.38M(-23%), 3.8B	61.0%(+3.0)	39.0%(+4.0)	7.2	118.6
Baseline + slim-neck, SPPF*4, CA*3, Mish, EIou *	1.38M(-23%), 3.8B	62.2%(+4.2)	41.5%(+6.5)	7.4	115.0

Table 4. The comparisons of the detectors based on slim neck and the originals of the different state-of-the-art lightweight detectors (PASCAL VOC 2007+12).

Detectors	Parameters number / FLOPs	mAP _{0.5}	mAP _{0.95}	Inference time _{b=1} (ms)	FPS
Originals:					
YOLOv3-tiny	8.71M, 13.0B	42.5%	18.5%	3.2	202.5
YOLOv4-tiny	6.11M, 17.6B	45.3%	21.3%	3.7	178.6

YOLOv5n	1.79M, 4.3B	58.0%	35.0%	5.8	136.8
MobileNetv3-YOLOv5s	3.59M, 6.4B	55.3%	32.6%	6.7	121.4
ShuffleNetv2-YOLOv5s	5.56M, 11.6B	56.1%	35.4%	5.0	151.3
GhostNet-YOLOv5s	3.73M, 8.2B	63.0%	42.1%	6.0	135.1
Slim neck by GSConv:					
slim-neck YOLOv3-tiny	5.86M, 9.6B	56.8%(+14.3)	33.6%(+15.1)	3.0	219.5
slim-neck YOLOv4-tiny	5.66M, 16.2B	61.3%(+16.0)	37.3%(+16.0)	3.7	179.1
slim-neck YOLOv5n	1.15M, 3.5B	58.9%(+0.9)	37.1%(+2.1)	4.8	155.4
GSConv-MobileNetv3-YOLOv5s	9.30M, 14.1B	61.9%(+6.6)	41.4%(+8.8)	8.3	102.9
GSConv-ShuffleNetv2-YOLOv5s	7.74M, 13.6B	58.7%(+2.6)	37.9%(+2.5)	5.8	137.1
GSConv-GhostNet-YOLOv5s	3.73M, 8.2B	63.6%(+0.6)	42.8%(+0.7)	6.8	122.8

Table 5. The performances of the slim-neck tiny detectors on the Jetson Nano (PASCAL VOC 2007+12).

Detectors	FLOPs	mAP _{0.5}	Inference time _{FP16, b=4}	FPS
slim-neck YOLOv3-tiny	9.6B	50.8%	30.1 ms	108.6
slim-neck YOLOv4-tiny	16.2B	56.8%	36.0 ms	91.4



Figure 11. The visual results of the slim-neck approach in the field traffic

5. Conclusions

To sum up, in this paper we introduce a new method, the GSConv, to allow the depth-wise separable convolutional to achieve the close effects to the standard convolutional and more efficient. And we design the one-shot aggregation module, VoV-GSCSP, to replace the ordinary bottleneck module to speed up inference. Further, we provide the slim-neck design paradigm for lightweight. In our experiments, the GSConv shows the better performance compared to the other lightweight convolutional methods. And with our approach, the tested detectors throw away 7.2%~32.7% of the computational cost but

obtain 1.2%~35.3% improvement of the accuracy and the given results outperform state-of-the-art detectors’.

Data Availability Statement:

Publicly available data sets:

1. The WiderPerson:
<http://www.cbsr.ia.ac.cn/users/sfzhang/WiderPerson/>
2. The PASCAL VOC 2012:
<http://host.robots.ox.ac.uk/pascal/VOC/voc2012/>
3. The SODA10M:
<https://soda-2d.github.io/index.html>

Appendix A. The comparisons of the FLOPs and parameters amount between the DSC and SC

The effect of DSC is obvious in the reduction of the parameters number of a model. The number of parameters for once conventional convolutional operation is $C_1 \times K_1 \times K_2 \times C_2$, and the number of parameters for a DSC operation is $C_1 \times K_1 \times K_2 + 1 \times 1 \times C_1 \times C_2$, where C_1 and C_2 are the number of channels of the feature maps from input and output, and $K_1 \times K_2$ is the kernel size of convolutional operation. The calculation cost of once conventional convolution operation is $W \times H \times C_1 \times K_1 \times K_2 \times C_2$, and the calculation cost of a DSC operation is $W \times H \times C_1 \times K_1 \times K_2 + W \times H \times 1 \times 1 \times C_1 \times C_2$, where W and H are the width and height of the feature maps from input and output. We can explain why DSC operation is cheaper than conventional convolutional by assuming the following conditions:

$$\left\{ \begin{array}{l} size_{input} = W \times H \times C_1 = 320 \times 320 \times 3 \\ size_{output} = W \times H \times C_2 = 320 \times 320 \times 16 \\ size_{kernel} = K_1 \times K_2 = 3 \times 3 \\ ratio_p = \frac{C_1 \times K_1 \times K_2 + 1 \times 1 \times C_1 \times C_2}{C_1 \times K_1 \times K_2 \times C_2} = \frac{1}{C_2} + \frac{1}{K_1 \times K_2} \approx 0.174 \\ ratio_c = \frac{W \times H \times C_1 \times K_1 \times K_2 + W \times H \times 1 \times 1 \times C_1 \times C_2}{W \times H \times C_1 \times K_1 \times K_2 \times C_2} \\ = \frac{1}{C_2} + \frac{1}{K_1 \times K_2} \approx 0.174 \end{array} \right.$$

where the $ratio_p$ is the ratio of the number of DSC and conventional convolution operation parameters, and the $ratio_c$ is the ratio of the calculation cost of them. Obviously, comparison between the DSC and SC, the parameters number and the calculation cost of the former are indeed less and much lower than latter.

References

1. R. Girshick; J. Donahue; T. Darrell; J. Malik. Rich feature hierarchies for accurate object detection and semantic segmentation. *in Proc. IEEE Comput. Soc. Conf. Comput. Vis. Pattern Recognit. (CVPR)*, Location of Conference, Country, Jun. 2014.
2. R. Girshick. Fast R-CNN. *Proc. IEEE Int. Conf. Comput. Vis. (ICCV)*, Dec. 2015.
3. S. Ren; K. He; R. Girshick; J. Sun. Faster R-CNN: Towards real-time object detection with region proposal networks. *IEEE Trans. Pattern Anal. Mach. Intel.*, vol. 39, no. 6, pp. 1137-1149, Jun. 2017.
4. J. Redmon; S. Divvala; R. Girshick; and A. Farhadi. You only look once: Unified, real-time object detection. *in Proc. IEEE Conf. Comput. Vis. Pattern Recog. (CVPR)*, pp 779-788, Jun. 2016.
5. J. Redmon; A. Farhadi. YOLO9000: better, faster, stronger. *in Proc. IEEE Conf. Comput. Vis. Pattern Recog. (CVPR)*, Jul. 2017, arXiv:1612.08242. [Online]. Available: <https://arxiv.org/abs/1612.-08242v1>
6. J. Redmon; A. Farhadi. YOLOv3: An incremental improvement. Apr. 2018, arXiv:1804.02767. [Online]. Available: <https://arxiv.org/abs/1804.02767>
7. A. Bochkovskiy; C. Y. Wang; H-Y. M. Liao. Yolov4: Optimal speed and accuracy of object detection. Apr. 2020, arXiv:2004.10934. [Online] Available: <https://arxiv.org/abs/2004.10934>
8. W. Liu; D. Anguelov; D. Erhan; C. Szegedy; Scott Reed; C. Y. Fu; A. C. Berg. SSD: Single shot multibox detector. *in Proc. Eur. Conf. Comput. Vis. (ECCV)*, Sep. 2016, pp. 21-37.
9. C. Y. Fu; W. Liu; A. Ranga; A. Tyagi; A. C. Berg. DssD: Deconvolutional single shot detector. Jan. 2017, arXiv:1701.06659. [Online]. Available: <https://arxiv.org/abs/1701.06659>
10. F. Chollet. Xception: Deep learning with depthwise separable convolutions. *in Proc. IEEE Conf. Comput. Vis. Pattern Recog. (CVPR)*, Oct. 2016, arXiv:1610.02357. [Online]. Available: <https://arxiv.org/abs/1610.02357v1>
11. A. G. Howard; M. Zhu; B. Chen; D. Kalenichenko; W. Wang; T. Weyand; M. Andreetto; A. Hartwig. Mobilenets: Efficient convolutional neural networks for mobile vision applications. Apr. 2017, arXiv:1704.04861. [Online]. Available: <https://arxiv.org/abs/1704.04861>
12. M. Sandler; A. Howard; M. Zhu; A. Zhmoginov; L. Chen. Mobilenetv2: Inverted residuals and linear bottlenecks. *in Proc. IEEE Conf. Comput. Vis. Pattern Recog. (CVPR)*, Jun. 2018, arXiv:1801.04381. [Online]. Available: <https://arxiv.org/abs/1801.-04381v4>
13. A. Howard; M. Sandler; G. Chu; L. Chen; B. Chen; M. Tan; W. Wang; Y. Zhu; R. Pang; V. Vasudevan; Q. V. Le; H. Adam. Searching for MobileNetV3. *in Proc. IEEE Int. Conf. Comput. Vis. (ICCV)*, Apr. 2019, arXiv:1704.04861. [Online]. Available: <https://arxiv.org/abs/1704.04861>
14. X. Zhang; X. Zhou; M. Lin; J. Sun. ShuffleNet: An extremely efficient convolutional neural network for mobile devices. *in Proc. IEEE Conf. Comput. Vis. Pattern Recog. (CVPR)*, Jul. 2017, arXiv:1707.01083. [Online]. Available: <https://arxiv.org/abs/1707.-01083v1>
15. N. Ma; X. Zhang; H. Zheng; J. Sun. ShuffleNet V2: Practical guidelines for efficient CNN architecture design. *in Proc. Eur. Conf. Comput. Vis. (ECCV)*, Jul. 2018, arXiv:1807.11164. [Online]. Available: <https://arxiv.org/abs/1807.11164v1>
16. K. Han; Y. Wang; Q. Tian; J. Guo; C. Xu; C. Xu. GhostNet: More features from cheap operations. *in Proc. IEEE Conf. Comput. Vis. Pattern Recog. (CVPR)*, Mar. 2020, arXiv:1911.11907. [Online]. Available: <https://arxiv.org/abs/1911.11907>
17. A. Krizhevsky; I. Sutskever; G. E. Hinton. ImageNet classification with deep convolutional neural networks. *Currant Associates, Inc.* vol. 25, 2012.
18. K. Simonyan; and A. Zisserman. Very deep convolutional networks for large-scale image recognition. Apr. 2015, arXiv:1409.1556. [Online]. Available: <https://arxiv.org/abs/1409.1556>
19. K. He; X. Zhang; S. Ren; J. Sun. Deep residual learning for image recognition. *in Proc. IEEE Conf. Comput. Vis. Pattern Recog. (CVPR)*, Jun. 2016, pp. 770-778.
20. Lin, T. Y., Dollár, P., Girshick, R., He, K., Hariharan, B., & Belongie, S. (2017). Feature pyramid networks for object detection. In Proceedings of the IEEE conference on computer vision and pattern recognition (pp. 2117-2125).
21. Tian, Z., Shen, C., Chen, H., & He, T. (2019). Fcos: Fully convolutional one-stage object detection. In Proceedings of the IEEE/CVF international conference on computer vision (pp. 9627-9636).
22. Zhu, C., He, Y., & Savvides, M. (2019). Feature selective anchor-free module for single-shot object detection. In Proceedings of the IEEE/CVF conference on computer vision and pattern recognition (pp. 840-849).
23. Neubeck A, Van Gool L. Efficient non-maximum suppression[C]//18th International Conference on Pattern Recognition (ICPR'06). IEEE, 2006, 3: 850-855.

24. Wang C Y, Bochkovskiy A, Liao H Y M. Scaled-yolov4: Scaling cross stage partial network[C]//Proceedings of the IEEE/cvf conference on computer vision and pattern recognition. 2021: 13029-13038.
25. K. He; X. Zhang; S. Ren; J. Sun. Spatial pyramid pooling in deep convolutional networks for visual recognition. *in IEEE Transactions on Pattern Analysis and Machine Intelligence*, vol. 37, no. 9, pp. 1904-1916, Sept. 2015.
26. J. Hu; L. Shen; S. Albanie; G. Sun; E. Wu. Squeeze-and-excitation networks. *in Proc. IEEE Conf. Comput. Vis. Pattern Recog. (CVPR)*, May. 2019, arXiv:1709.01507. [Online]. Available: <https://arxiv.org/abs/1709.01507v4>
27. S. Woo, J. Park; J. Lee; I. S. Kweon. CBAM: Convolutional block attention module. *in Proc. Eur. Conf. Comput. Vis. (ECCV)*, Jul. 2018, arXiv:1807.06521. [Online]. Available: <https://arxiv.org/abs/1807.06521v1>
28. Q. Hou, D. Zhou; J. Feng. Coordinate attention for efficient mobile network design. *in Proc. IEEE Conf. Comput. Vis. Pattern Recog. (CVPR)*, Jun. 2021, arXiv:2103.02907. [Online]. Available: <https://arxiv.org/abs/2103.02907>
29. Huang G, Liu Z, Van Der Maaten L, et al. Densely connected convolutional networks[C]//Proceedings of the IEEE conference on computer vision and pattern recognition. 2017: 4700-4708.
30. Lee Y, Hwang J, Lee S, et al. An energy and GPU-computation efficient backbone network for real-time object detection[C]//Proceedings of the IEEE/CVF Conference on Computer Vision and Pattern Recognition Workshops. 2019: 0-0.
31. Wang C Y, Liao H Y M, Wu Y H, et al. CSPNet: A new backbone that can enhance learning capability of CNN[C]//Proceedings of the IEEE/CVF conference on computer vision and pattern recognition workshops. 2020: 390-391.
32. J. Yu; Y. Jiang; Z. Wang; Z. Cao; T. Huang. UnitBox: An advanced object detection network. In *Proceedings of the 24th ACM international conference on Multimedia*, pp. 516-520, Oct. 2016.
33. H. Rezatofighi; N. Tsoi; J. Gwak; A. Sadeghian; I. Reid; S. Savarese. Generalized intersection over union: A metric and a loss for bounding box regression. *in Proc. IEEE Conf. Comput. Vis. Pattern Recog. (CVPR)*, Jun. 2019, pp. 658-666.
34. Z. Zheng; P. Wang; W. Liu; J. Li; R. Ye; D. Ren. Distance-IoU Loss: Faster and better learning for bounding box regression. In *Proceedings of the AAAI Conference on Artificial Intelligence (AAAI)*, vol. 34, No. 07, pp. 12993-13000, Apr. 2020.
35. Z. Zheng; P. Wang; D. Ren; W. Liu; R. Ye; Q. Hu; W. Zuo. Enhancing geometric factors in model learning and inference for object detection and instance segmentation. *in IEEE Transactions on Cybernetics*, Aug. 2021, pp. 1-13, doi: 10.1109/TCYB.2021.3095305.
36. Y. Zhang; W. Ren; Z. Zhang; Z. Jia; L. Wang; T. Tan. Focal and efficient IoU loss for accurate bounding box regression. Jan. 2021, arXiv:2101.08158 2021. [Online]. Available: <https://arxiv.org/abs-/2101.08158>
37. P. Ramachandran; B. Zoph; Q. V. Le. Searching for activation functions. Oct. 2017, arXiv:1710.05941. [Online]. Available: <https://arxiv.org/abs/1710.05941>
38. D. Misra. Mish: A self regularized non-monotonic activation function. Aug. 2020, arXiv:1908.08681. [Online]. Available: <https://arxiv.org/abs/1908.08681>
39. X. Glorot; A. Bordes; Y. Bengio. Deep sparse rectifier neural networks. *Proceedings of the fourteenth international conference on artificial intelligence and statistics*, vol. 15, pp. 315-323, Apr. 2011.
40. S. Zhang; Y. Xie; J. Wan; H. Xia; S. Z. Li; G. Guo. WiderPerson: A diverse dataset for dense pedestrian detection in the wild. *in IEEE Transactions on Multimedia*, vol. 22, no. 2, pp. 380-393, Feb. 2020, doi: 10.1109/TMM.2019.2929005.
41. M. Everingham; J. Winn. The PASCAL visual object classes challenge 2012 (VOC2012) development kit. *Pattern Anal., Stat. Model. Comput. Learn., Tech. Rep.* 8, 2011, p. 5.
42. Han J, Liang X, Xu H, et al. Soda10m: Towards large-scale object detection benchmark for autonomous driving[J]. arXiv e-prints, 2021: arXiv: 2106.11118.